Steps in H_2 Oxidation on Rh: OH Desorption at High Temperatures†

M. P. Zum Mallen, W. R. Williams,‡ and L. D. Schmidt*

Department of Chemical Engineering and Materials Science, University of Minnesota, Minneapolis, Minnesota 55455

Received: April 27, 1992

The desorption of OH radicals over a polycrystalline Rh foil exposed to mixtures of H_2, O_2, and H_2O for surface temperatures between 1000 and 1800 K is measured by laser-induced fluorescence (LIF) and used to determine the elementary steps in H_2 oxidation on Rh. The results on Rh are compared to previous results obtained on Pt. OH desorption maxima and apparent OH desorption activation energies are slightly lower in H_2 oxidation on Rh compared to on Pt. However, hydroxyl desorption in H_2O decomposition and its influence by O_2 on Rh is markedly different than on Pt. Whereas O_2 addition gives a monotonic increase in radical desorption asymptotically approaching a maximum on Pt, O_2 addition enhances radical desorption only at low pressures on Rh. At high O_2 pressures, the OH desorption rate decreases with additional O_2. Modeling indicates that these differences are caused by the high activation energy for oxygen desorption on Rh and the resulting high coverage of O. Consequently, OH is a much less stable surface species on Rh than on Pt. The 12-step mechanism for reversible H_2 oxidation used to model the results on Pt is modified to allow for 2 types of O binding sites on Rh—competitive and noncompetitive sites, with the latter probably being a surface oxide. Simulation of the $H_2O + O_2$ experiments allows us to determine the equilibrium between the two types of O sites.

Introduction

We have previously used laser-induced fluorescence (LIF) coupled with mass spectrometry to determine the steps in high-surface-temperature oxidation of H_2 on Pt.[1] In this paper, we continue the investigation of the H_2 oxidation mechanism through a comparable study on Rh, which has catalytic properties similar to Pt. Because the same surface species exist over these two metals, the reaction mechanism of H_2 oxidation on Rh is virtually identical to that on Pt, although the kinetic parameters differ considerably. The mechanism and notation used are

$$H_{2(g)} \underset{k_{dH}}{\overset{k_{aH}}{\rightleftarrows}} 2H_{(a)} \qquad (H)$$

$$O_{2(g)} \underset{k_{dO}}{\overset{k_{aO}}{\rightleftarrows}} 2O_{(a)} \qquad (O)$$

$$H_2O_{(g)} \underset{k_{dW}}{\overset{k_{aW}}{\rightleftarrows}} H_2O_{(a)} \qquad (W)$$

$$OH_{(a)} \overset{k_{dOH}}{\rightarrow} OH^*_{(g)} \qquad (OH)$$

for rates of adsorption/desorption and

$$H_{(a)} + O_{(a)} \underset{k_{-1}}{\overset{k_1}{\rightleftarrows}} OH_{(a)} \qquad (1)$$

$$H_{(a)} + OH_{(a)} \underset{k_{-2}}{\overset{k_2}{\rightleftarrows}} H_2O_{(a)} \qquad (2)$$

$$2OH_{(a)} \underset{k_{-3}}{\overset{k_3}{\rightleftarrows}} H_2O_{(a)} + O_{(a)} \qquad (3)$$

for the surface reactions.

We will show that most of the significant differences between Pt and Rh are due mainly to differences in oxygen adsorption. Whereas oxygen adsorbs on Pt in only one binding state with a desorption activation energy of 52 kcal/mol,[2] oxygen adsorbs on Rh in two binding states with activation energies of 25 and 85 kcal/mol.[3] At high temperatures, one should therefore expect much higher coverages of O on Rh relative to Pt.

On Pt, H_2 oxidation at high temperature is controlled primarily by flux limitations rather than surface-site limitations. On Rh, however, oxygen surface coverage approaches a monolayer at 0.1 Torr of O_2, even at high surface temperatures. Therefore, combustion kinetics on Rh can be limited by the availability of surface sites as well as the flux of a reactant.

Conversely, adsorption and dissociation of hydrogen and H_2O on Rh are quite similar to Pt. Hydrogen adsorbs in one binding state on Rh with an activation energy of 18 kcal/mol,[4] the same activation energy as for Pt.[5] H_2O has a 10.8 kcal/mol desorption activation energy over both Rh and Pt.[6,7]

Although OH desorption from Pt has been studied extensively, very little work has been done on OH desorption from Rh. The exception is a survey of OH desorption from H_2 oxidation over various noble metals by Ljungström et al.[8] They reported that Rh gives significantly less OH desorption than Pt. They also measured an activation energy of 25 kcal/mol for OH desorption from Rh in H_2 oxidation, but they did not show any data to support this value.

As mentioned earlier, this study parallels our previous study of H_2 oxidation on Pt.[1] We shall first show the measured OH desorption rates and partial pressures for both the forward reaction of H_2 oxidation and the reverse reaction of H_2O decomposition. These experimental results will be compared to the results on Pt. Next, a model simulation of the experimental results will be presented. Finally, the agreement between model and experiment will be discussed, and the kinetic parameters obtained will be compared with those in the literature.

Results

The experimental apparatus has been described in detail in a previous paper.[1] Briefly, all reactions occurred in a mechanically pumped flow system containing a resistively heated 0.17- × 3.0-cm Rh foil suspended by nickel leads. The total pressure was measured with a capacitance manometer, and partial pressures

* To whom correspondence should be addressed.
† This research is partially supported by DOE under Grant DE-FGO2-88ER13878-AO2.
‡ Current address: Du Pont Central Research and Development, Experimental Station, Wilmington, DE 19880-0262.

0022-3654/58/2097-0625$04.00/0

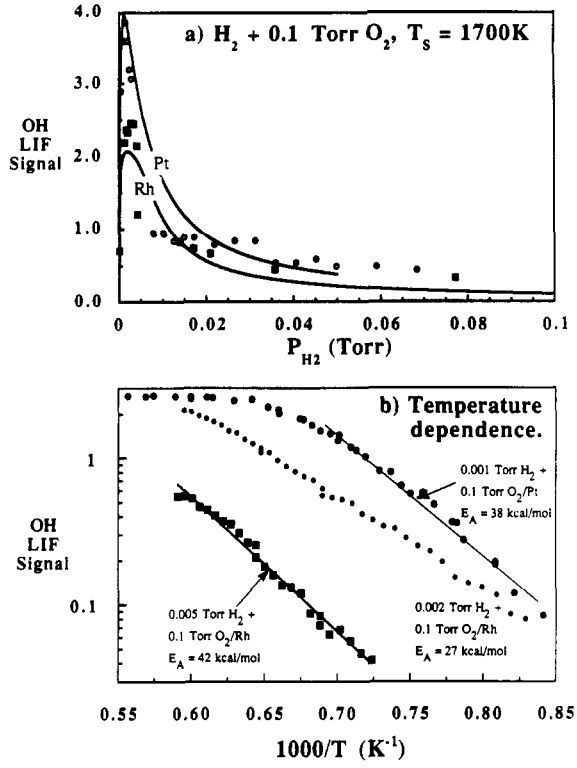

Figure 1. (a) Comparison of results for H_2 oxidation on Pt and Rh foils. Lines indicate weighted average fits to experimental data. (b) Comparison of experimental (points) and model results (lines) for OH desorption as a function of reciprocal T_s for 0.005 Torr of H_2 + 0.1 Torr of O_2 (■) on Rh and 0.001 Torr of H_2 + 0.1 Torr of O_2 on Pt (○); and experimental results for 0.002 Torr of H_2 + 0.1 Torr of O_2 (●) on Rh. The model fails to accurately predict activation energy on the H_2 lean side of the OH desorption peak.

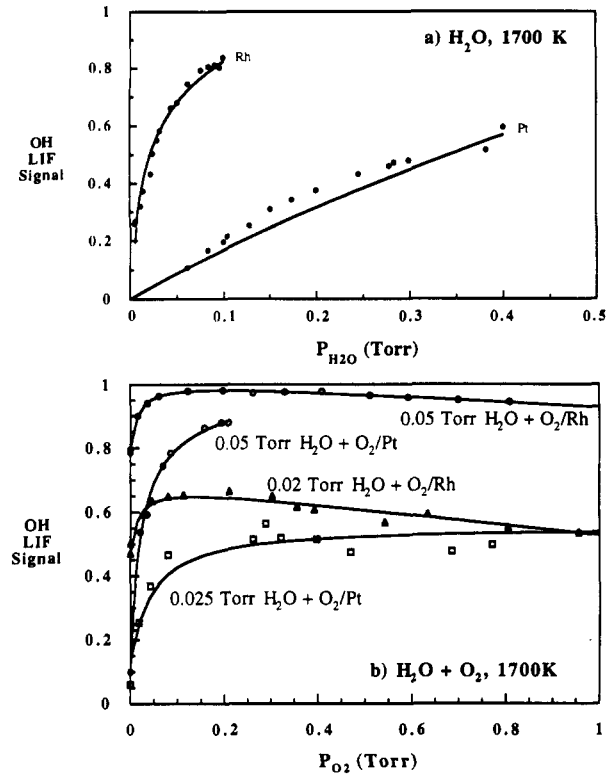

Figure 2. Comparison of results on Pt and Rh for H_2O decomposition (a) and H_2O + O_2 (b).

in the reacting systems were determined by a mass spectrometer. In nonreacting systems and for calibrations, partial pressures were determined from differences in capacitance manometer measurements. The OH radical was detected by saturating the Q_11 rotational line of the $^2A\Sigma^+ = {}^2X\Pi$ (307.844-nm[9]) transition with a Nd:YAG pumped dye laser. The fluorescence signal was filtered and detected with a photomultiplier and a boxcar integrator.

Although the OH desorption rates have arbitrary units, we estimate that a LIF signal of unity corresponds to $\sim 1 \times 10^{16}$ molecules/(cm^2 s). The relative numbers are comparable to within ±10% in all figures and in our previous results because the LIF OH transition was saturated.

With the exception of Figures 1a and 2 where the Pt and Rh results are compared, all points in the following figures are experimental results, while *all curves represent model results from fits to be described later.*

$H_2 + O_2$. The OH desorption rate as a function of H_2 pressure for a constant inlet O_2 feed ($P^i_{O_2}$ = 0.1 Torr) over 1700 K Rh and Pt surfaces is compared in Figure 1a. The OH desorption rate from Rh is about half that from Pt at 1700 K, but the qualitative features from Pt and Rh are quite similar. Specifically, a sharp OH maximum occurs for lean H_2/O_2 mixtures (3×10^{-3} Torr of H_2 in ~0.1 Torr of O_2 at 1700 K). This is followed by a long tail in which significant OH desorption still occurs in excess H_2. The H_2O formation rate (not shown) first increases rapidly and then becomes constant for all H_2 pressures beyond the OH maximum.

A comparison of the temperature dependences of OH desorption for H_2 oxidation on Rh and Pt is shown in Figure 1b. The figure illustrates the results for 0.002 and 0.005 Torr of H_2 in 0.1 Torr of O_2 on Rh as well as 0.001 Torr of H_2 in 0.1 Torr of O_2 on Pt. We also compare this to model results. Similar to Pt, two activation energies were observed for OH desorption: an activation energy of 27 kcal/mol for OH desorption on the fuel lean side of the OH desorption peak, in agreement with Ljungström et al.,[8] and an activation energy of 42 kcal/mol on the rich side of the OH desorption peak. Unlike Pt, however, the OH desorption rate on Rh did not become temperature independent at high temperatures for either composition. Thus, Pt appeared to be become flux limited at temperatures above ~1400 K, while Rh does not up to at least 1700 K (Figure 1b).

H_2O Decomposition. Isothermal measurements of OH desorption rates for the decomposition of H_2O as a function of H_2O pressure over a Rh foil are compared to Pt at 1700 K in Figure 2a. Model fits are shown at various temperatures in Figure 4a. We also determined the effects of H_2 addition (Figure 5a) and O_2 addition (Figure 2b—with Pt results, Figure 6a and 6b—with model fits) on the decomposition of H_2O on Rh at various temperatures. The overall production of H_2 and O_2 from these mixtures was negligible (conversions < 1%) in all experiments (through 1700 K) as determined by monitoring m/e = 2 and 32 with the mass spectrometer.

Unlike Pt, where OH desorption had a nearly linear dependence on H_2O pressure, the dependence of OH desorption on H_2O pressure on Rh appears to have a fractional order (Figure 4a). OH radical desorption rates are higher from Rh than from Pt (Figure 2a), in contrast to H_2 oxidation where the reverse is observed. The addition of H_2 to H_2O decomposition (Figure 5a) causes a strong decrease in OH signal. This is similar to the results on Pt and can be fit by the expression[1]

$$[OH] = \frac{[OH]_0}{1 + AP_{H_2}} \tag{4}$$

The effect of O_2 addition on OH desorption during H_2O decomposition on Rh is markedly different from that on Pt (Figure 2b). When OH desorption is measured vs O_2 pressure for varying H_2O pressures at 1700 K (Figure 6a) and for varying temperatures for 0.025 Torr of H_2O (Figure 6b), the data are not accurately fit by the analytic expression used for Pt. Rather than a monotonic

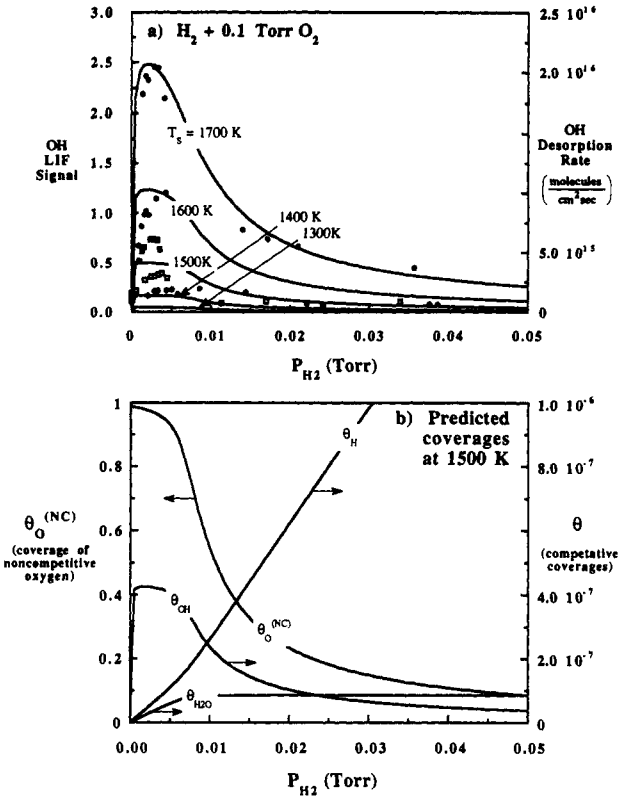

Figure 3. (a) Comparison of experimental (points) and model results (lines) for OH desorption as a function of H_2 pressure added to a constant $P^i_{O_2}$ = 0.1 Torr over 1300 K (◆), 1400 K (□), 1500 K (■), 1600 K (○), and 1700 K (●) Rh surfaces. (b) Model predictions of surface coverages as a function of H_2 pressure added to a constant $P^i_{O_2}$ = 0.1 Torr over a 1500 K Rh surface.

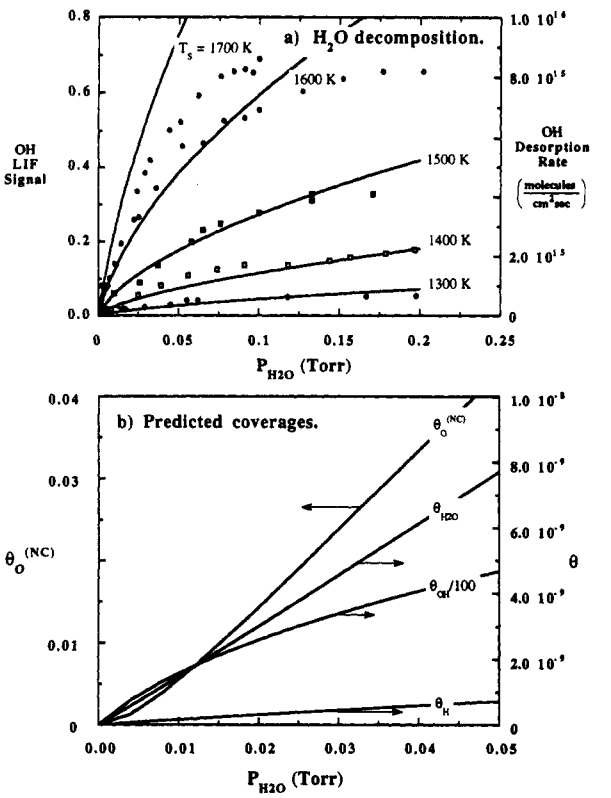

Figure 4. (a) Comparison of experimental (points) and model results (lines) for OH desorption during H_2O decomposition over 1300 K (◆), 1400 K (□), 1500 K (■), 1600 K (○), and 1700 K (●) Rh surfaces. (b) Model predictions of surface coverages during H_2O decomposition over 1700 K Rh.

increase in OH signal with increasing O_2 pressure, a decay in the OH signal is observed for higher O_2 pressures. Therefore, the expression must be modified to account for this decay. As a first approximation, adding a linear decay in O_2 worked quite well:

$$[OH] = [OH]_0 + \frac{BP_{O_2}}{1 + CP_{O_2}} - DP_{O_2} \qquad (5)$$

where B, C, and D are constants. We shall show later that these fractional forms are obtained from simple models of this process.

Model

We first attempted to model this system with the identical model which was successful for hydrogen oxidation on Pt,[1] using new parameters for the surface reactions on Rh. The mechanism and nomenclature are given in the Introduction.

However, on Rh, high O coverages exist due to its high heat of desorption. If one assumes competitive adsorption, as assumed on Pt, oxygen can now block sites available to react at these temperatures and therefore completely block all reactions. Model results assuming competitive adsorption predict apparent OH desorption activation energies approaching 100 kcal/mol, in sharp disagreement with the experimental result of 42 kcal/mol. These high activation energies are a direct consequence of the blocking of O adatoms. The reaction becomes limited by the desorption of oxygen, which has two binding states with desorption activation energies of 25 and 85 kcal/mol.[3] Therefore, we had to assume that O adsorption was at least partially noncompetitive with the other adsorbates.

Mass Balance Equations. The model was therefore modified to allow for two types of sites, those available for O (designated with $\theta_O^{(NC)}$, for noncompetitive adsorption) and those available for other species (designated as θ). The species equations therefore become

$$d\theta_O^{(NC)}/dt = 0 = 2k_{aO}(\theta_V^{(NC)})^n P_{O_2} + k_{-1}\theta_{OH}\theta_V^{(NC)} + k_3\theta_{OH}^2\theta_V^{(NC)} - nk_{dO}(\theta_O^{(NC)})^n - k_1\theta_H\theta_O^{(NC)} - k_{-3}\theta_{H_2O}\theta_O^{(NC)}\theta_V \qquad (6)$$

$$d\theta_H/dt = 0 = 2k_{aH}\theta_V^n P_{H_2} + k_{-1}\theta_{OH}\theta_V^{(NC)} + k_{-2}\theta_{H_2O}\theta_V - nk_{dH}\theta_H^n - k_1\theta_H\theta_O^{(NC)} - k_2\theta_H\theta_{OH} \qquad (7)$$

$$d\theta_{OH}/dt = 0 = k_1\theta_H\theta_O^{(NC)} + k_{-2}\theta_{H_2O}\theta_V + 2k_{-3}\theta_{H_2O}\theta_O^{(NC)}\theta_V - k_{-1}\theta_{OH}\theta_V^{(NC)} - k_2\theta_H\theta_{OH} - 2k_3\theta_{OH}^2\theta_V^{(NC)} - k_{dOH}\theta_{OH} \qquad (8)$$

$$d\theta_{H_2O}/dt = 0 = k_{aW}\theta_V P_{H_2O} + k_2\theta_H\theta_{OH} + k_3\theta_{OH}^2\theta_V^{(NC)} - k_{dW}\theta_{H_2O} - k_{-2}\theta_{H_2O}\theta_V - k_{-3}\theta_{H_2O}\theta_O^{(NC)}\theta_V \qquad (9)$$

where the coverage of vacant sites θ_V is

$$\theta_V = 1 - \theta_H - \theta_{OH} - \theta_{H_2O} \qquad (10)$$

and the coverage of vacant sites for noncompetitive oxygen $\theta_V^{(NC)}$ is

$$\theta_V^{(NC)} = 1 - \theta_O^{(NC)} \qquad (11)$$

While this model fit experimental data quite well in the H_2 + O_2, H_2O, and H_2O + H_2 systems, no choice of parameters could predict the decrease in OH signal at high pressures observed in the H_2O + O_2 system (Figure 6a and 6b). It seems clear that this feature is due to partial blocking of O. Therefore, an oxygen

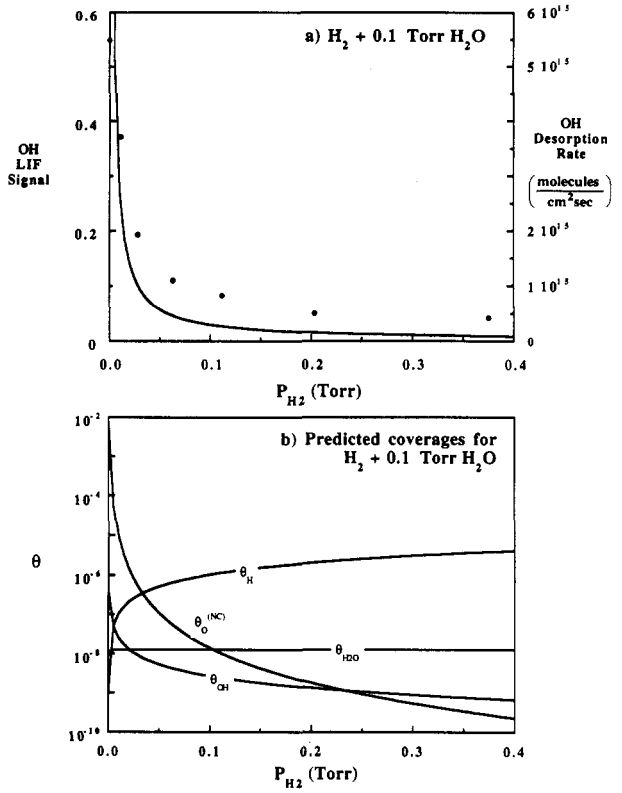

Figure 5. (a) Comparison of experimental (points) and model results (lines) for OH desorption as a function of H_2 pressure added to 0.1 Torr of H_2O over a 1900 K Rh surface. (b) Model predictions of surface coverages as a function of H_2 pressure added to 0.1 Torr of H_2O over 1900 K Rh.

binding state ratio, f, was introduced:

$$f = \frac{\theta_O}{\theta_O^{(NC)}} \tag{12}$$

This variable defines the ratio of competitively to noncompetitively adsorbed oxygen and modifies eq 10 as follows:

$$\theta_V = 1 - \theta_H - f\theta_O^{(NC)} - \theta_{OH} - \theta_{H_2O} \tag{13}$$

Using a constant for the oxygen binding state ratio was still not adequate because the model predicted either a monotonically increasing or decreasing OH signal as a function of O_2 pressure for low and high values of f, respectively (Figure 7a). It was clear that f increased with O coverage and that a break in the curve occurred at $f \sim 0.25$.

The simplest mechanism to yield increasing blocking with increasing coverage is to assume that O in noncompetitive sites is in equilibrium with O in competitive sites:

$$O_{(a,NC)} + v \underset{}{\overset{K_{O(a)}}{\rightleftarrows}} O_{(a)} + v_{(NC)}; \quad K_{O(a)} < 1 \tag{14}$$

where v indicates a vacant surface site and $v_{(NC)}$ indicates a noncompetitive oxygen vacant surface site. Assuming the coverages of all species except oxygen are small, the equilibrium can be written as

$$K_{O(a)} = \frac{\theta_O(1 - \theta_O^{(NC)})}{\theta_O^{(NC)}(1 - \theta_O)} \tag{15}$$

We then solve for the coverage of competitive sites θ_O in terms of noncompetitive sites and obtain f as a function of $\theta_O^{(NC)}$:

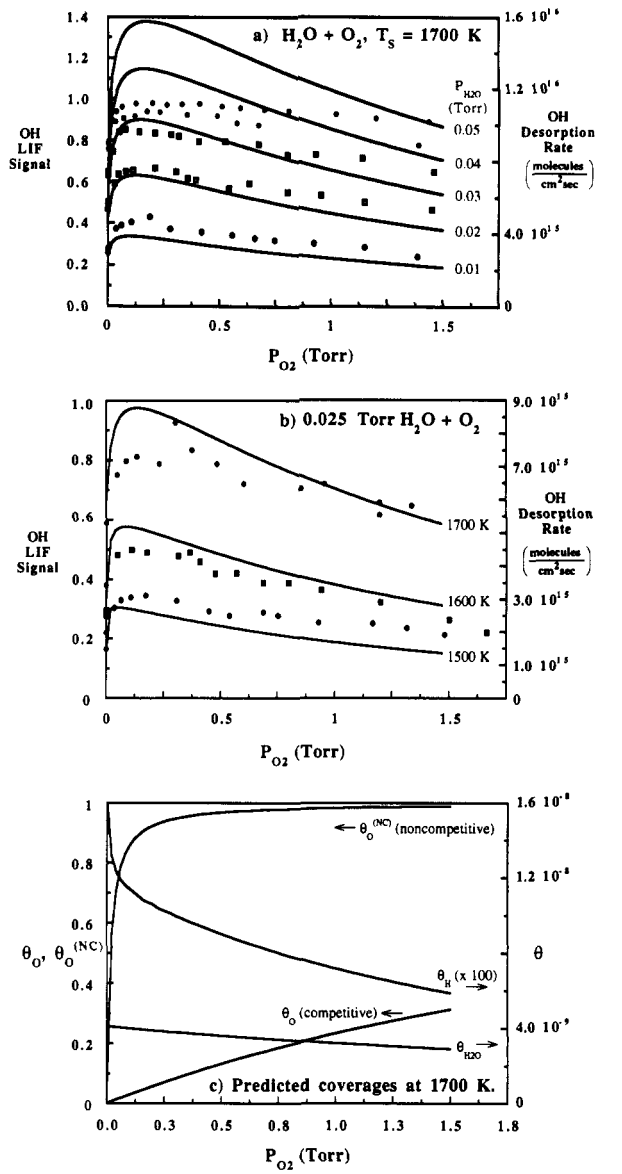

Figure 6. (a) Comparison of experimental (points) and model results (lines) for OH desorption as a function of O_2 pressure added to 0.01 Torr (◆), 0.02 Torr (□), 0.03 Torr (■), 0.04 Torr (○), and 0.05 Torr (●) of H_2O over a 1700 K Rh surface. (b) Comparison of experimental (points) and model results (lines) for OH desorption as a function of O_2 pressure added to 0.025 Torr of H_2O over 1500 K (◆), 1600 K (■), and 1700 K (○) Rh surfaces. (c) Model predictions of the surface coverages of H, H_2O, competitive O, and noncompetitive O as a function of O_2 pressure added to 0.025 Torr of H_2O over a 1700 K Rh surface.

$$\theta_O = \frac{K_{O(a)}\theta_O^{(NC)}}{1 - (1 - K_{O(a)})\theta_O^{(NC)}}$$

$$f = \frac{\theta_O}{\theta_O^{(NC)}} = \frac{K_{O(a)}}{1 - (1 - K_{O(a)})\theta_O^{(NC)}} \tag{16}$$

The oxygen binding state ratio and coverage of competitive oxygen obtained by fitting these results are plotted as a function of the coverage of noncompetitive oxygen for various K's in Figures 7b and 7c.

The variable oxygen binding state ratio in the model gave excellent fits for the $H_2O + O_2$ system, as will be shown in the following section. Moreover, since all other experiments were conducted at lower O_2 pressures, the assumption of no blocking rather than variable blocking had no effect on the model results for the $H_2 + O_2$, H_2O, and $H_2O + H_2$ systems.

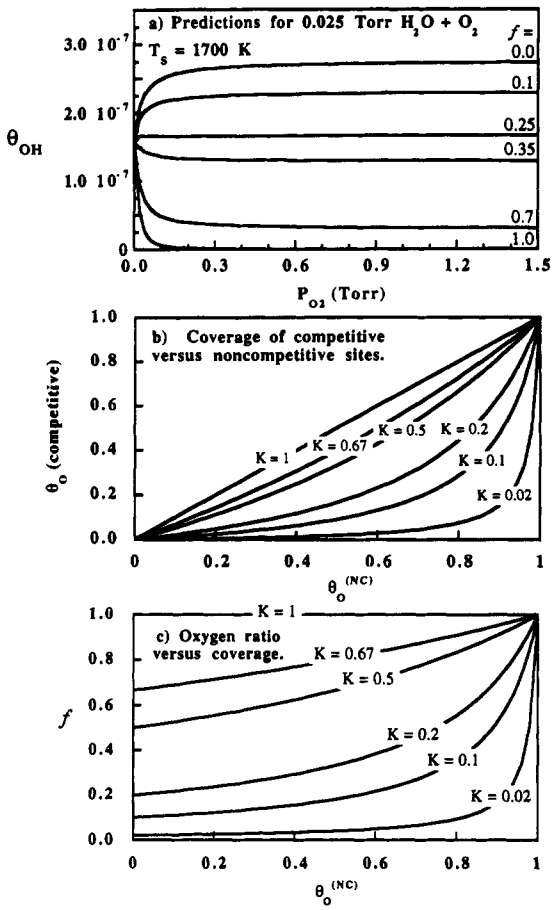

Figure 7. (a) Predicted coverages of OH as a function of O_2 pressure added to 0.025 Torr of H_2O over 1700 K Rh using a constant oxygen binding state ratio, f. (b) Coverage of competitive O vs noncompetitive O for various K's. (c) Oxygen binding state ratio as a function of noncompetitive O for various K's.

Numerical Results and Comparison with Experiments. The predicted results of OH desorption from the numerical solutions are shown as curve fits to the experimental results in Figures 1b, 3a, 4a, 5a, 6a, and 6b. Also, the predicted coverages of all surface species are shown in Figures 3b, 4b, 5b, and 6c. The rate parameters used for this fit are summarized and compared to our Pt results in Table I. All surface reaction and desorption rate constants have units of s^{-1}, and the adsorption rates have units of $Torr^{-1}\ s^{-1}$ because mass balances are in monolayer coverages.

Most of the surface reaction rate constants were obtained by fitting the model to the experimental data. Since the desorption kinetics of H_2, O_2, and H_2O are well-known in the literature, we treat these as fixed parameters. For the desorption rate of O_2, we averaged the 85 and 25 kcal/mol binding sites based on the relative coverages of these two surface species at saturation.[3] The adsorption rates based on the gas kinetic theory are given by

$$k_{ai} = \frac{S_i}{(2\pi m R T_g)^{1/2}} \tag{17}$$

The sticking coefficients are listed along with the actual adsorption rates in Table I.

Since most experiments were isothermal, we used literature values where available for the activation energies of the surface reactions as initial guesses, and some activation energies were also fixed by thermodynamic constraints. However, since there is considerably less data available for Rh than for Pt, most of the activation energies were determined by fitting the experimental isothermal results taken at various temperatures. Having determined the activation energies for both forward and reverse reactions, we can obtain a complete potential energy diagram for the $H_2 + O_2$ reaction (Figure 8a).

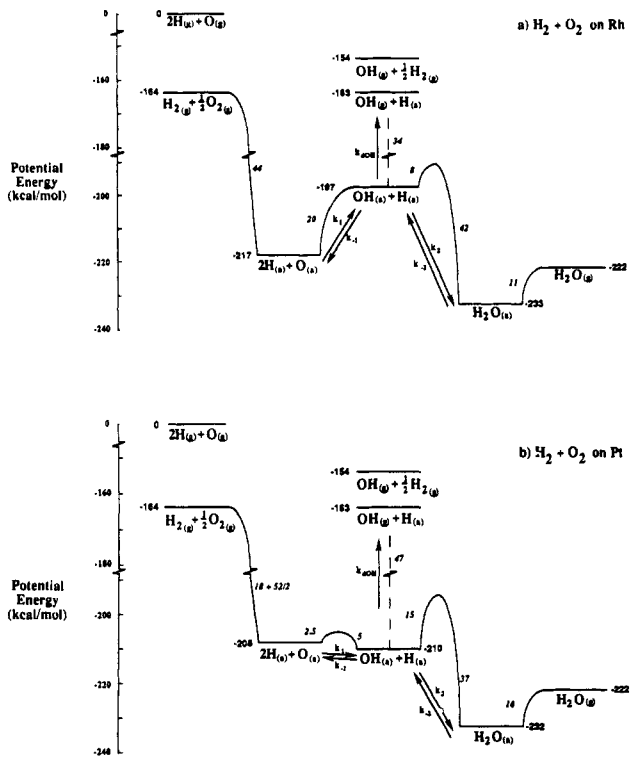

Figure 8. Comparison of results on Rh (a) and Pt (b) for the potential energy diagram of the reaction pathway $H_{2(g)} + {}^1/_2O_{2(g)} \rightarrow H_2O_{(g)}$.

H_2 Oxidation. The model curve fits in the $H_2 + O_2$ system are fairly good (Figure 3a). The model gives the experimentally observed relative maximum OH desorption signals at the higher surface temperatures as well as the experimentally observed tail for higher H_2 pressures. For lower temperatures, the experimental results continue to exhibit rather sharp peaks, whereas the model predicts that peaks will exhibit breaks. The plot of surface coverages vs H_2 pressure at T_S = 1500 K shown in Figure 3b indicates that this coincides with a high, relatively invariant O coverage at low H_2 pressures.

Plots of the temperature dependence of the OH signal during H_2 oxidation (Figure 1b) show that the model predicts the apparent activation energy of OH desorption observed for H_2/O_2 mixtures on the H_2-rich side of the OH desorption peak. However, the model failed to accurately predict the lower activation energy observed on the lean side of the peak, although it did predict a slightly lower activation energy at high T_S. We believe that this discrepancy is due to broadening of the OH desorption peak at the lower surface temperatures (Figure 3a).

Table II summarizes model sensitivity to OH and H_2O desorption during the $H_2 + O_2$ reaction. These data were calculated by changing the preexponential factor for a particular reaction step and calculating the resulting change in product desorption. Specifically, the sensitivity is defined here as

$$\text{sensitivity} = \frac{\Delta r/r}{\Delta k_i/k_{io}} \tag{18}$$

where r is the rate of desorption (molecules/(cm^2 s)) and k_i is the varied parameter (the reaction rate preexponentials). Calculations were performed at 1700 and 1300 K under both fuel-rich and lean conditions (both sides of the desorption peak in Figure 3a). Sensitivities were not calculated for negligible reaction steps (k_{-1} and k_{-3}).

H_2O Decomposition. The experiments and the model agree quite well for H_2O decomposition, particularly at lower surface temperatures (Figure 4a). Both model and experiment show a fractional order dependence of OH vs H_2O pressure. However, the model shows a slightly higher order in P_{H_2O} than the experimental results. Rh probably gives a larger OH signal than

TABLE I: Rate Constants for Models of Rh and Pt

reaction		rhodium preexponential, $torr^{-1}\ s^{-1}$ (s^{-1})	rhodium activation energy, kcal/mol	refs	platinum (Williams et al.[1]) preexponential, $torr^{-1}\ s^{-1}$ (s^{-1})	platinum (Williams et al.[1]) activation energy, kcal/mol
$H + O \xrightarrow{k_1} OH$	(1)	7×10^{12}	20	Wagner and Schmidt[10]	1×10^{15}	2.5
$OH \xrightarrow{k_{-1}} H + O$	(-1)	-	0	this work	1×10^{8}	5
$H + OH \xrightarrow{k_2} H_2O$	(2)	3×10^{17}	8	this work	9×10^{16}	15
$H_2O \xrightarrow{k_{-2}} H + OH$	(-2)	5×10^{14}	42	this work	1.8×10^{13}	37
$2OH \xrightarrow{k_3} H_2O + O$	(3)	4×10^{15}	15 24	this work Gurney and Ho[11]	1×10^{15}	12.3
$H_2O + O \xrightarrow{k_{-3}} 2OH$	(-3)		63	thermodynamic constraints	-	31
$H_{2(g)} \xrightarrow{k_{aH}} H_{(a)}$	(H)	4.5×10^5 ($s_H = 0.32$)	0	this work	1.4×10^6 ($s_H = 1.0$) 1.5×10^5 ($s_H = 0.105$)	0 0
$H_{(a)} \xrightarrow{k_{dH}} H_{2(g)}$	(-H)	1×10^{13}	18	Yates et al.[4]	1×10^{13}	18
$O_{2(g)} \xrightarrow{k_{aO}} O_{(a)}$	(O)	3.5×10^5 ($s_O = 1$)	0	Root et al.[3]	1×10^4 ($s_O = 0.04$)	0
$O_{(a)} \xrightarrow{k_{dO}} O_{2(g)}$	(-O)	1×10^{13}	70	Wagner and Schmidt,[10] Root et al.[3]	1×10^{13}	52
$H_2O_{(g)} \xrightarrow{k_{aW}} H_2O_{(a)}$	(W)	7.4×10^4 ($s_W = 0.16$)	0	this work	5×10^4 ($s_W = 0.1$)	0
$H_2O_{(a)} \xrightarrow{k_{dW}} H_2O_{(g)}$	(-W)	1×10^{13}	10.8	Kiss and Solymosi,[6] Wagner and Moylan[12]	1×10^{13}	10.8
$OH_{(a)} \xrightarrow{k_{dOH}} OH_{(g)}$	(OH)	8.1×10^{11}	34	this work	1.5×10^{13}	48
$O_{(a,NC)} + v \underset{K_{O(a)}}{\rightleftarrows} O_{(a)} + v_{(NC)}$		1×10^6	65	this work		

Pt because of its lower OH desorption energy. At low surface temperatures, the Rh OH signal tends to remain flat with increased H_2O pressure, possibly indicating that increases in adsorbed OH further dissociate via the energetically favorable reaction -1 route.

Hydrogen addition causes a sharp decrease in the OH signal (Figure 5a), and the model and experiments agree quite well for this system. Rh and Pt give almost identical OH desorption profiles for this system, and Figure 5b indicates that H_2 has the same effect on water decomposition on Rh as on Pt: H_2 addition increases the coverage of H which consumes the OH by shifting the equilibrium reactions 2 and -2 toward H_2O.

Predictions of O_2 addition on OH yields in H_2O decomposition using the variable oxygen binding state ratio are also quite good. Using a value of $K_{O(a)} = 0.005$ gave good fits for the isothermal results at 1700 K, particularly for 0.01, 0.02, and 0.03 Torr of H_2O decomposition (Figure 6a). For the $H_2O + O_2$ experiments conducted at 1600 and 1500 K, we found that values of $K_{O(a)} = 0.001$ and 0.0004 gave the best fits (Figure 6b). Since we expect that there would be some energy associated with the equilibrium between the two oxygen sites, we fit the temperature dependence of $K_{O(a)}$ to an Arrhenius expression giving the values shown in Table I. The calculated activation energy for $K_{O(a)}$ of 65 kcal/mol corresponds approximately to the difference in the oxygen desorption activation energies of 85 and 25 kcal/mol on Rh reported by Root et al.[3]

Figure 6c indicates that initially O adatoms consume the H adatoms to form OH via reaction -2. In addition to forming more OH, this also lowers the H coverage, shifting the equilibrium reactions 2 and -2 toward OH production. These two factors cause a rapid increase in OH production upon addition of O_2. At higher O_2 pressures, the O coverage becomes high enough that O starts to populate competitive sites blocking H_2O adsorption, which in turn decreases the OH coverage.

Discussion

Although H_2 oxidation on Rh is quite similar to H_2 oxidation on Pt, there are some important differences. These differences are almost entirely due to the dramatically different nature of the O adsorbate on Rh compared to Pt. The high activation energy of O desorption has many consequences on the reaction pathway for H_2 oxidation:

First, on the potential energy diagram for Rh (Figure 8a), this means that the 2H + O energy level is lower than the OH + H level, in contrast to Pt (Figure 8b) where the reverse is true.[1] This forces the OH formation from H and O, reaction 1, to be highly activated on Rh. This in turn makes the activation energy for H_2O formation from 2H + O on Rh much higher than on Pt.[10,13,14]

Next, coverages of O are nearly a monolayer on Rh, even for high surface temperatures, but on Pt, O coverages were typically around 10^{-5} at 1700 K. Therefore, whereas on Pt the kinetics are generally oxygen flux limited, oxygen on Rh can block the surface to adsorption, making some reactions limited by the availability of sites, particularly the $H_2O + O_2$ reaction.

The final and perhaps most interesting result of these two types of oxygen sites is the unique result for the $H_2O + O_2$ system where increasing the oxygen pressures initially increases OH desorption, but at high pressures, oxygen decreases OH desorption rates. As noted above, this strongly suggests that there is an equilibrium between the two types of sites, one noncompetitive and the other competitive with the other species. It further requires that the equilibrium favor the noncompetitive sites and that there is a $K_{O(a)}$ equilibrium activation energy, which indicates that the more strongly adsorbed binding state is noncompetitive.

TABLE II: Model Sensitivity to OH and H_2O Desorption[a]

reaction		0.002 Torr H_2 + 0.1 Torr O_2 (fuel lean)				0.01 Torr H_2 + 0.1 Torr O_2 (fuel rich)			
		1700 K		1300 K		1700 K		1300 K	
		r_{dOH}	r_{dW}	r_{dOH}	r_{dW}	r_{dOH}	r_{dW}	r_{dOH}	r_{dW}
$H + O \xrightarrow{k_1} OH$	(1)	0.93	0.63	0.99	0.66	0.33	0.27	0.15	0.11
$OH \xrightarrow{k_{-1}} H + O$	(-1)	–	–	–	–	–	–	–	–
$H + OH \xrightarrow{k_2} H_2O$	(2)	1.1	4.8×10^{-2}	1.2	0.56	1.2	9.2×10^{-3}	1.2	2.2×10^{-4}
$H_2O \xrightarrow{k_{-2}} H + OH$	(-2)	7.6×10^{-2}	4.7×10^{-3}	5.5×10^{-3}	$<10^{-5}$	8.4×10^{-2}	1.0×10^{-3}	5.4×10^{-3}	$<10^{-5}$
$2OH \xrightarrow{k_3} H_2O + O$	(3)	1.5×10^{-2}	4.4×10^{-3}	1.3×10^{-4}	$<10^{-5}$	3.0×10^{-3}	5.0×10^{-4}	$<10^{-5}$	$<10^{-5}$
$H_2O + O \xrightarrow{k_{-3}} 2OH$	(-3)	–	–	–	–	–	–	–	–
$H_{2(g)} \xrightarrow{k_{aH}} H_{(a)}$	(H)	2.5×10^{-2}	1.0	9.2×10^{-3}	1.0	1.1	0.40	1.5	0.20
$H_{(a)} \xrightarrow{k_{dH}} H_{2(g)}$	(-H)	8.2×10^{-3}	0.73	6.1×10^{-3}	0.69	0.78	0.22	0.94	8.4×10^{-2}
$O_{2(g)} \xrightarrow{k_{aO}} O_{(a)}$	(O)	0.21	9.4×10^{-2}	9.0×10^{-3}	1.8×10^{-3}	0.20	0.15	7.1×10^{-2}	5.1×10^{-2}
$O_{(a)} \xrightarrow{k_{dO}} O_{2(g)}$	(-O)	0.18	0.07	5.1×10^{-4}	7.9×10^{-5}	0.15	0.11	6.3×10^{-4}	4.4×10^{-4}
$H_2O_{(g)} \xrightarrow{k_{aW}} H_2O_{(a)}$	(W)	7.1×10^{-2}	0.94	5.2×10^{-3}	0.94	7.9×10^{-2}	0.94	5.2×10^{-3}	0.94
$H_2O_{(a)} \xrightarrow{k_{dW}} H_2O_{(g)}$	(-W)	9.4×10^{-2}	5.9×10^{-3}	6.9×10^{-3}	$<10^{-5}$	0.10	1.2×10^{-3}	6.9×10^{-3}	$<10^{-5}$
$OH_{(a)} \xrightarrow{k_{dOH}} OH_{(g)}$	(OH)	0.95	4.9×10^{-2}	1.0	8.7×10^{-4}	0.99	1.0×10^{-2}	1.0	2.2×10^{-4}
$O_{(a,NC)} + v \overset{K_{O(a)}}{\rightleftharpoons} O_{(a)} + v_{(NC)}$		3.2×10^{-3}	4.2×10^{-2}	$<10^{-5}$	3.7×10^{-3}	3.0×10^{-3}	4.7×10^{-3}	$<10^{-5}$	$<10^{-5}$

[a] Note that parameter sensitivities apply to the forward (H_2 + O_2) reaction only. Negligible reaction rates in the model (indicated with a dash) were not analyzed.

This is in remarkable agreement with previous work on oxygen adsorption on Rh and H_2 oxidation on Rh. First, Root et al.[3] showed, using TPD, that the 85 kcal/mol binding state populated first, followed by population of the 25 kcal/mol binding state at high coverages. Second, TPD results from Wagner and Schmidt[10] found that when oxygen is adsorbed only in the 85 kcal/mol binding state, H_2 adsorption is not blocked, but when oxygen is adsorbed in both binding states, significant blocking of H_2 adsorption occurs. Finally, assuming desorption energies of 25 and 85 kcal/mol for the two types of O sites predicts that $K_{O(a)}$ should have an activation energy of 85–25 = 60 kcal/mol, which is quite close to our value of 65 kcal/mol.

Therefore, we can associate O adsorbed in $\theta^{(NC)}$ sites with more strongly adsorbed O adatoms which do not block the reaction. Oxygen adsorbed in θ sites would be associated with more weakly bound oxygen and would compete with the other adsorbates. This also explains why such behavior is not observed on Pt, since there is only one oxygen binding state, and its desorption activation energy is small enough so that no significant site blocking occurs at high surface temperature.[2]

Another major difference between H_2 oxidation on Rh and on Pt is due to the nature of the OH adsorbate species itself. As can be seen in the potential energy diagram (Figure 8a), OH is quite unstable on Rh. The activation energy to form OH via reaction 1 is much greater than that to consume OH via reaction 2. OH can therefore be viewed as strictly a transition state between H and O and H_2O adsorbates rather than as a well-defined stable species.

Finally, we compare the other parameter values with those in the literature. In contrast to Pt, few of these intermediate steps have been studied. Values have been reported for the OH formation reaction (1) and the OH recombination reaction (3). Only Gurney and Ho have obtained results for the activation energy of OH recombination reaction (3), and they report a value of 24 kcal/mol for this reaction in very good agreement with our value of 15 kcal/mol. Furthermore, our model was fairly insensitive to the choice of this value, and it is quite possible that the actual value for this activation energy is greater than 15 kcal/mol.

As for reaction 1 on Rh, although our energy value of 20 kcal/mol is in agreement with that of Wagner and Schmidt,[10] others using FEM, EELS, and LEED to monitor the surface have reported lower values of 2–5 kcal/mol.[4,11,15] However, these values were based on H_2 titration of O precovered surfaces, and Yates et al.[4] note that these experiments could actually be measuring the activation energy of H_2 adsorption. We also showed this in a previous paper.[1]

Summary

These experiments further demonstrate the ability to probe the kinetics of high-temperature surface reactions by monitoring OH desorption. We have also shown that by fitting the LIF data to a comprehensive model, we can examine other adsorbates and reactions indirectly. The examination of the effect of O_2 on H_2O decomposition has allowed us to confirm previous results concerning the nature of the O adsorbate[3,10] and to determine the equilibrium expression which governs the amount of O adsorbed in each of the two binding states.

This study also shows that despite the many similarities between Pt and Rh, there are sharp differences between the two surfaces. Most of these differences arise from the strong adsorption of O on Rh. This strong bond has the potential for making oxygen behave almost as a poison on the Rh surface, but it apparently does not completely block the surface to adsorption of other species. However, this has the effect of altering the potential energy diagram to make OH formation, and consequently water formation, a much more activated process on Rh compared to on Pt. As a result, since water formation occurs in all combustion reactions, one should expect that most catalytic combustion reactions would be faster and have lower activation energies on

Pt than on Rh. Experiments to probe steps in other fuel oxidation reactions are currently in progress.

Nomenclature

k_{aH}, k_{aO}, k_{aW}	adsorption rate constants for H_2, O_2, and H_2O ($Torr^{-1}$ s^{-1})
E_A	activation energy
s_H, s_O, s_W	zero coverage sticking coefficients for H_2, O_2, and H_2O
k_{dH}, k_{dO}, k_{dW}, k_{dOH}	desorption rate constants for H, O, H_2O, and OH (s^{-1})
r_{dOH}, r_{dW}	desorption rates for OH and H_2O (molecules/(cm^2 s))
$K_{O(a)}$	equilibrium constant between competitive and noncompetitive $O_{(a)}$
k_i, k_{-i}	rate constant of forward and reverse reaction i (s^{-1})
P_{H_2}, P_{O_2}, P_{H_2O}	CSTR pressures of H_2, O_2, and H_2O with reaction
[OH]	experimental OH signal
$[OH]_0$	experimental OH signal for H_2O with no O_2 or H_2 present
T_S	surface temperature
θ	surface coverage (competitive)
$\theta^{(NC)}$	surface coverage (noncompetitive)
f	oxygen binding state ratio

References and Notes

(1) Williams, W. R.; Marks, C. M.; Schmidt, L. D. *J. Phys. Chem.* **1992**, *96*, 5922.
(2) Matsushima, T. *Surf. Sci.* **1985**, *157*, 297.
(3) Root, T. W.; Schmidt, L. D.; Fisher, G. B. *Surf. Sci.* **1983**, *134*, 30–45.
(4) Yates, J. T.; Thiel, P. A.; Weinberg, W. H. *Surf. Sci.* **1979**, *84*, 427–439.
(5) McCabe, R. W.; Schmidt, L. D. *Surf. Sci.* **1977**, *65*, 189.
(6) Kiss, J.; Solymosi, F. *Surf. Sci.* **1986**, *177*, 191–206.
(7) Fisher, G. B.; Gland, J. L. *Surf. Sci.* **1980**, *94*, 446.
(8) Ljungström, S.; Hall, J.; Kasemo, B.; Rosén, A.; Wahnström, T. *J. Catal.* **1987**, *107*, 548–556.
(9) Dieke, G. H.; Crosswhite, H. M. *J. Quant. Spectrosc. Radiat. Transfer* **1962**, *2*, 97–199.
(10) Wagner, M. L.; Schmidt, L. D. *J. Phys. Chem.*, to be published.
(11) Gurney, B. A.; Ho, W. *J. Chem. Phys.* **1987**, *87*, 5562–5577.
(12) Wagner, F. T.; Moylan, T. E. *Surf. Sci.* **1987**, *191*, 121–146.
(13) Kwasniewski, V. J.; Schmidt, L. D. *J. Phys. Chem.* **1992**, *96*, 5938.
(14) Ogle, K. M.; White, J. M. *Surf. Sci.* **1986**, *169*, 425.
(15) Gorodetskii, V. V.; Nieuwenhuys, B. E.; Sachtler, W. M. H.; Boreskov, G. K. *Appl. Surf. Sci.* **1981**, *7*, 355–371.